

Slim-neck by GSConv: A better design paradigm of detector architectures for autonomous vehicles

Hulin Li^{1*}, Jun Li², Hanbing Wei², Zheng Liu³, Zhenfei Zhan² and Qiliang Ren¹

¹ College of Traffic and Transportation, Chongqing Jiaotong University, Chongqing 400074, China;

² School of Mechatronics and Vehicle Engineering, Chongqing Jiaotong University, Chongqing 400074, China;

³ School of Engineering, University of British Columbia, Okanagan, Kelowna BC V1V 1V7, Canada;

* Correspondence Author

alanli@mails.cqjtu.edu.cn (H.L.); cqleejun@cqjtu.edu.cn (J.L.); hbwei@cqjtu.edu.cn (H.W.);

zheng.liu@ubc.ca (Z.L.); zhenfeizhan@cqjtu.edu.cn (Z.Z); qlren@cqjtu.edu.cn (Q.R.)

Abstract

Object detection is a significant downstream task in computer vision. For the on-board edge computing platforms, a giant model is difficult to achieve the real-time detection requirement. And, a lightweight model built from a large number of the depth-wise separable convolution layers cannot achieve the sufficient accuracy. We introduce a new lightweight convolution technique, GSConv, to lighten the model but maintain the accuracy. The GSConv accomplishes an excellent trade-off between the model's accuracy and speed. And, we provide a design paradigm, slim-neck, to achieve a higher computational cost-effectiveness of the detectors. The effectiveness of our approach was robustly demonstrated in over twenty sets comparative experiments. In particular, the detectors of ameliorated by our approach obtains state-of-the-art results (e.g. 70.9% mAP_{0.5} for the SODA10M at a speed of ~ 100FPS on a Tesla T4 GPU) compared with the originals. Code is available at <https://github.com/alanli1997/slim-neck-by-gsconv>

Keywords: GSConv; object detection; design paradigm; lightweight; autonomous driving

1. Introduction

Object detection is a fundamental perception capability required for driverless cars. Currently, detection algorithms by deep learning dominate the field. These algorithms are of two types in terms of detection stages: the one-stage [1-3, 24, 43] and the two-stage [4-9]. The two-stage detectors perform better in the detection of small objects and get higher mean average precision (mAP) by the principle of sparse detection, but these detectors all come at the cost of speed. The one-stage detectors are not as effective as two-stage detectors in the detection and localization of small objects, but they are faster than the latter on work, which is very important for industry. But this state is changing with the application of Transformer in the computer vision field. The intuitive understanding from brain-like research is that the model with more neurons gain a stronger nonlinear expression ability. But what should not be neglected is that the powerful ability and low energy consumption of the biological brains to process information are beyond the computers far. The strong model cannot build by simply increasing the number of model parameters endlessly. The lightweight design is effective to mitigate high computational costs at the current stage. This purpose is mostly accomplished by using the depth-wise separable convolution (DSC) operations to reduce the amounts of parameters and floating-point-operations (FLOPs, the number of multiply-adds), and the effect is obvious, details in Appendix. However, the disadvantages of the DSC are also obvious: the channel information of the input image is separated in the calculation process. **Figure 1 (a) and (b)** show the calculation process of the vanilla convolution (SC, the standard convolution) and the

DSC. This deficiency results the DSC in a much lower feature extraction and fusion capability than the SC.

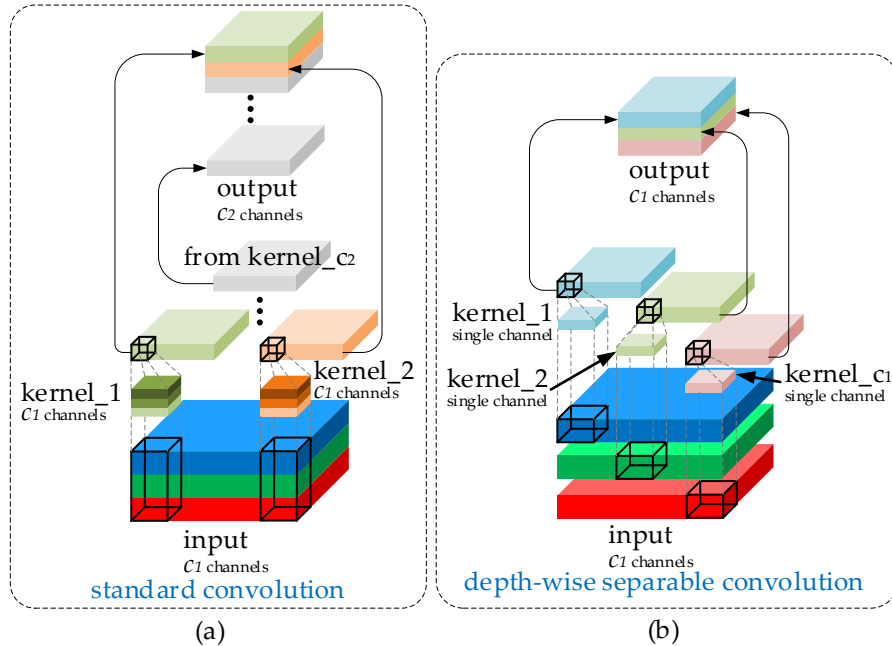


Figure 1. The calculation process of the (a) SC and the (b) DSC. The SC is the channel-dense convolution computation and the DSC is the channel-sparse convolution computation.

For self-driving cars, the speed is as important as the accuracy. The previous lightweight works, such as Xception [10], MobileNets [11-13] and ShuffleNets [14-15], improved the detector speed greatly by the DSC operations. But the lower accuracy of these models is worrying when these models are applied to the autonomous vehicles. In fact, these works propose some methods to alleviate this inherent flaw (also the peculiarity) of the DSC: MobileNets use a large number of $1*1$ dense convolutions to fuse the channels information that is computed independently; ShuffleNets use the “channel shuffle” to enable the interaction of channels information and GhostNet [16] uses the “halved” SC operations to retain the interaction information between channels. But, the $1*1$ dense convolutions take up more computational resources instead, the effect of using “channel shuffle” still does not touch the results of the SC and the GhostNet is more or less back on the road to the SC, influences may come from many aspects. Many lightweight models use the similar thinking to design the basic architecture: only use the DSC from the very beginning to end of the deep neural networks. But the DSC’s flaw is directly amplified in the backbone, whether this is used for image classification or detection. We believe that **the SC and the DSC can be cooperative**. We note that the feature maps generated by only shuffling the output channels of the DSC are still the “depth-wise separated”. In order to make the outputs of the DSC as close as possible to the SC, we introduce a new method—a mix convolution with SC, DSC and a shuffle, named GSConv. As show in Figure 2, we use the shuffle to permeate the information generated by the SC (the channel-dense convolution operations) into every part of the information generated by the DSC. The shuffle is a uniform mixing strategy. This method allows the information from the SC to be fully mixed into the outputs of the DSC by uniformly to exchange local feature information on different channels, without bells and whistles. Figure 3 shows the visualization results of the SC, DSC and GSConv. The GSConv’s feature maps are significantly more similar to the SC’s than the DSC’s is to the SC’s. On the lightweight models, we obtain a significant accuracy improvement by only using the GSConv layers to replace the SC layers; On other models, when we use the SC in the backbone and use the GSConv in the neck (slim-neck), the accuracy of the model is very close to the original; And if we add a few tricks, the accuracy and speed of the model surpass the original model. The slim-neck with GSConv method minimizes the negative impact of the DSC’s flaw on the models and to utilize the benefits of the DSC efficiently. The main contributions of ours can be summarized as follows:

- 1) We introduce a new lightweight convolution method, the GSConv. This method makes the outputs of the convolutional calculation as close to the SC's as possible, and reduces the computational cost;
- 2) We provide a design paradigm, the slim-neck with a standard backbone, for the detector architecture of self-driving cars;
- 3) We verified the effectiveness of different widely used tricks on the GSConv-Slim-Neck Detectors, which can be a reference for study in this field.

The rest of the article is organized as follows: we give a brief overview of some relevant works and methods about the lightweight and performance improvement of detectors in Section 2, and provide the details of our study in Section 3, our experimental results presented in Section 4, all the work analyzed with a discussion in Section 5 and summarized with a final conclusion in Section 6.

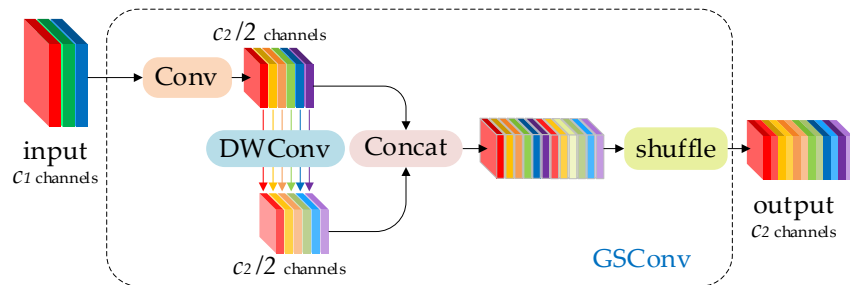


Figure 2. The structure of the GSConv module. The “Conv” box consists of three layers: a convolutional-2D layer, a batch normalization-2D layer, and an activation layer. The “DWConv” marked in blue here means the DSC operation.

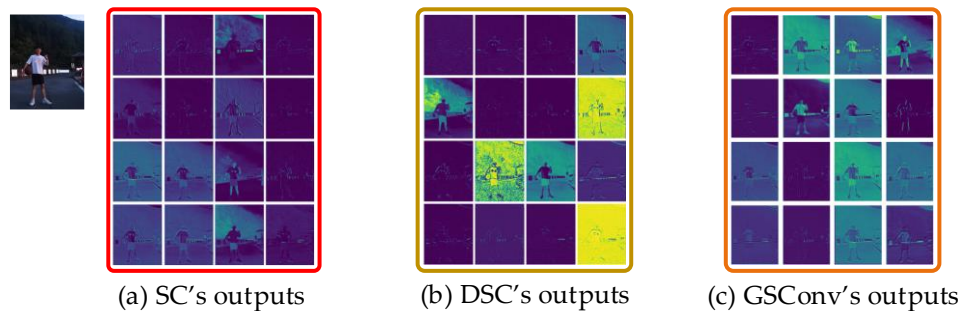


Figure 3. The features in the 2nd layer of the YOLOv5n: (a) The features generated by the SC operation; (b) The features generated by the DSC operation; (c) The features generated by the GSConv operation.

2. Related Work

Usually, a detector based on the convolutional neural networks (CNNs) consists of three parts, a backbone, a neck and a head. The backbone for the extraction features of the input, the neck for allocation and merging features better to the head, and the head detects the objects by materials from the neck. For the backbone, AlexNet [17] demonstrated the powerful feature extraction ability of CNNs. Then, the backbone of detectors or classifiers started to be designed using the SC, such as VGG [18], ResNet [19] and DarkNet [6-7]. However, these “bulky” models are very unfriendly to edge computing devices. In terms of model structure design, researchers have proposed classic lightweight models such as MobileNet, ShuffleNet, and GhostNet for edge devices. For the neck, FPN [20] improves the speed and accuracy of object detection models by independently performing prediction operations on different scale feature map layers. For the head, the main difference is that the model uses anchor-based [1-3, 5-9, 24] or anchor-free [21-22] methods to accomplish objects localization tasks. The former may be more controllable for designers and users, but the NMS [23] must be used to filter out the prediction box with the highest IoU threshold score. The latter is more flexible and no more parameters can be controlled manually, but this also leads to an increase in instability of the model. The choice of anchor-based or anchor-free is not the focus of this paper, but it is worth noting that the SOTA models are still using the anchor-based method currently. More, the attention mechanisms, such as SPP [25], SE [26], CBAM [27] and CA [28], can

improve the efficiency and performance of detectors, especially for the lightweight detectors. We can obtain the better cost performance by a proper use of these modules, and the relevant details are described in Section 3.

3. Materials and Methods

The details of our work will be described in this section. We aim to build a simple and efficient neck for the detectors to apply in the autonomous vehicles. Therefore, many factors such as convolution method, feature fusion structure, computational efficiency, computational cost effectiveness and many other factors are taken into considerations.

3.1 Why GSConv

In order to speed up the computation of predictions in the end, the fed images in CNNs almost always have to undergo a similar transformation process in the backbone: the spatial information is transferred step by step toward the channels. And each time the spaces (the width and height) compression and channels expansion of the feature maps will cause a partial loss of semantic information. The channel-dense convolutional computation maximally preserves the hidden connections between each channel, but the channel-sparse convolution severs these connections completely. The GSConv preserves these connections as much as possible with lower time complexity. Generally, the time complexity of convolutional computation is defined by FLOPs. Therefore, the time complexity (without bias) of the SC (channel-dense convolution), DSC (channel-sparse convolution) and GSConv is:

$$Time_{sc} \sim O(W \cdot H \cdot K_1 \cdot K_2 \cdot C_1 \cdot C_2), \quad Time_{dsc} \sim O(W \cdot H \cdot K_1 \cdot K_2 \cdot 1 \cdot C_2), \quad \text{and} \quad Time_{GSConv} \sim O[W \cdot H \cdot K_1 \cdot K_2 \cdot \frac{C_2}{2} (C_1 + 1)],$$

where the W is the width of the output feature map; H is the height of the output feature map; $K_1 \cdot K_2$ is the size of the convolution kernel; C_1 is the number of channels per convolution kernel, and also the number of channels of the input feature map and C_2 is the number of channels of the output feature map. In [Table 3](#), we compare the contribution of five different convolution blocks (SC, DSC, ShuffleNet method, GhostNet method and the GSConv method) to the performance of the model.

We want to complete the shuffle in GSConv in the simpler way possible and without additional FLOPs. One option is to mix features evenly by transposition operating and then reconstruct them to the original size [\[14\]](#), which is a way without additional FLOPs, but is strictly a non-standard operation (may be unsupported on some devices). Another option is to use linear operations for the shuffle task, which costs less, but it is canonical and supported by all devices capable of performing convolution computations. The ablation study on the performance of the two shuffle methods are reported in [Table 4](#). The advantages of the GSConv are more evident for lightweight detectors, which benefits from the enhanced nonlinear expression capability through the addition of a DSC layer and a shuffle. But if the GSConv be used at all stages of the model, the model's network layers will be deeper and these deep layers will aggravate the resistance to data flow and increase the inference time significantly. When these feature maps come to the neck, they have become slender enough (the channel dimension reaches the maximum, and the width and height dimensions reach the minimum) and the transformations have become moderate. Therefore, the better choice is to use the GSConv in the neck only (slim-neck + standard backbone). At this stage, using the GSConv to process the concatenated feature maps is just right: redundant repetitive information is less and compressed not needed, and the attention modules works better, such as the SPP and the CA.

3.2 The slim-neck

We investigate the generalized methods to enhance the learning ability of CNNs, such as DensNet [\[29\]](#), VoVNet [\[30\]](#) and CSPNet [\[31\]](#), and then design the structure of slim-neck on the theory of these methods. We design the slim neck to reduce the computational complexity and inference time of the detector but maintain the accuracy. The GSConv accomplishes the task of reducing the computational complexity, and the task of reducing the inference time and maintaining the accuracy requires new models.

3.2.1 The element modules of the slim-neck

The computational cost of GSConv is about 50% ($0.5+0.5C_l$, the larger the C_l value, the closer the ratio is to 50%) of the SC, but its contribution to the model learning ability is comparable to the latter. Based on GSConv, we continue to introduce the GS bottleneck on the basis of the GSConv, and Figure 4 (a) shows the structure of the GS bottleneck module. Then, we use the one-shot aggregation method to design the cross stage partial network (GSCSP) module, VoV-GSCSP. Figure 4 (b), (c) and (d) show the three design schemes we provided for the VoV-GSCSP, respectively, where (b) is simple and straightforward and faster inference, and (c) and (d) have a higher reuse rate for the features. In fact, the simpler structure modules are more likely to be used because of the hard-ware-friendly. Table 5 reports the results of the ablation study in detail for the three structures of VoV-GSCSP_{1, 2, 3}, and indeed, VoV-GSCSP₁ shows a higher performance-to-price ratio. Finally, we need the flexibility to use the four modules, the GSConv, the GS bottleneck, and the VoV-GSCSP. We can build the slim-neck layers like to put together Legos.

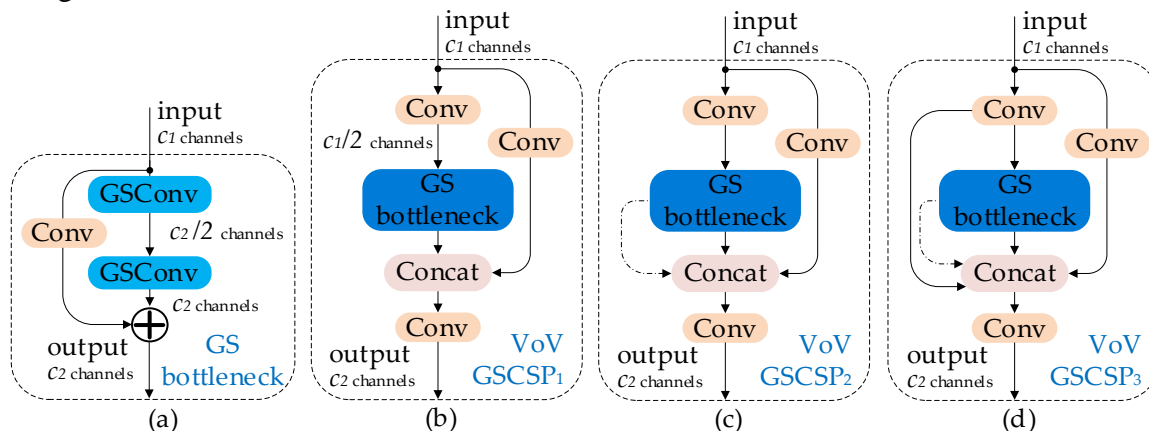


Figure 4. The structures of the (a) GS bottleneck module and the (b), (c), (d) VoV-GSCSP_{1, 2, 3} modules

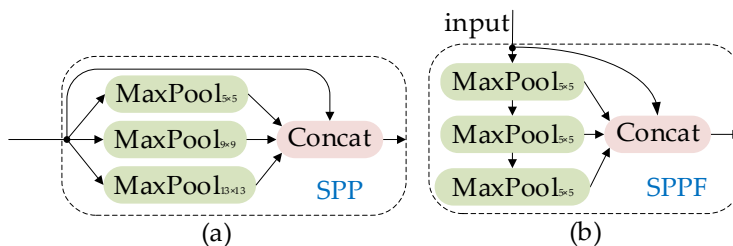


Figure 5. The structures of the (a) SPP module and (b) SPPF module. The SPPF's output is the same as SPP's with more computationally efficient.

3.2.2 The slim-neck for the YOLO family

The YOLO family detectors are more widely used in the industry because of the efficient detection. We use the element modules of the slim-neck to retrofit the neck layers for the Scaled-YOLOv4l [24] and YOLOv5l [43]. Table 1 and 2 show the comparisons between the slim framework and the native framework of the two detectors.

Table 1. The neck architectures of slim neck scaled yolov4 and the original

Slim neck architecture			Original neck architecture*		
Layers in Neck	In/out-put channels	Param.	Layers in Neck	In/out-put channels	Param.
0. P5 -> SPPF (1/32)	1024 / 512	1.575M	0. P5 -> SPPCSP (1/32)	1024 / 512	7.611M
1. GSConv+Upsample	512 / 256	0.069M	1. Conv+Upsample	512 / 256	0.132M
2. P4 -> Conv (1/16)	512 / 256	0.130M	2. P4 -> Conv (1/16)	512 / 256	0.132M
3. Concat 1. & 2.	512	-	3. Concat 1. & 2.	512	-
4. VoV-GSCSP ₁ ×2	512 / 256	0.220M	4. CSP	512 / 256	0.986M

5. GSConv+Upsample	256 / 128	0.018M	5. Conv+Upsample	256 / 128	0.033M
6. P3 -> Conv (1/8)	256 / 128	0.033M	6. P3 -> Conv (1/8)	256 / 128	0.033M
7. Concat 5. & 6.	256	-	7. Concat 5. & 6.	256	-
8. VoV-GSCSP ₁ ×2	256 / 128	0.056M	8. CSP	256 / 128	0.247M
9. GSConv ×2	128 / 256	0.323M	9. Conv ×2	128 / 256	0.592M
10. Concat 3. & 9.	512	-	10. Concat 3. & 9.	512	-
11. VoV-GSCSP ₁ ×2	512 / 256	0.220M	11. CSP	512 / 256	0.986M
12. GSConv ×2	256 / 512	2.361M	12. Conv ×2	256 / 512	2.361M
13. Concat 0. & 12.	1024	-	13. Concat 0. & 12.	1024	-
14. VoV-GSCSP ₁ ×2	1024 / 512	0.865M	14. CSP	1024 / 512	3.938M
15. GSConv	512 / 1024	2.374M	15. Conv	512 / 1024	4.721M

Table 2. The neck architectures of slim neck yolov5l and the original

Slim neck architecture			Original neck architecture*		
Layers in Neck	I/O channels	Param.	Layers in Neck	I/O channels	Param.
0. P5 -> SPPF (1/32)	1024 / 1024	2.625M	0. P5 -> SPPF (1/32)	1024 / 1024	2.625M
1. GSConv+Upsample	1024 / 512	0.269M	1. Conv+Upsample	1024 / 512	0.525M
2. Concat P4 & 1. (1/16)	1024	-	2. Concat P4 & 1. (1/16)	1024	-
3. VoV-GSCSP ₁ ×3	1024 / 512	0.903M	3. C3 ×3	1024 / 512	2.758M
4. GSConv+Upsample	512 / 256	0.069M	4. Conv+Upsample	512 / 256	0.132M
5. Concat P3 & 4. (1/8)	512	-	5. Concat P3 & 4. (1/8)	512	-
6. VoV-GSCSP ₁ ×3	512 / 256	0.230M	6. C3 ×3	512 / 256	0.691M
7. GSConv	256 / 256	0.298M	7. Conv	256 / 256	0.590M
8. Concat 4. & 7.	512	-	8. Concat 4. & 7.	512	-
9. VoV-GSCSP ₁ ×3	512 / 512	0.641M	9. C3 ×3	512 / 512	2.495M
10. GSConv	512 / 512	1.187M	10. Conv	512 / 512	2.360M
11. Concat P5 & 10.	1024	-	11. Concat P5 & 10.	1024	-
12. VoV-GSCSP ₁ ×3	1024 / 1024	2.527M	12. C3 ×3	1024 / 1024	9.972M

3.3 The improvement tricks for free

We can use some local feature enhancement methods in CNNs-based detectors with simple structure and low computational cost. These enhancement methods, attention mechanisms, can significantly improve the model accuracy, but are much cheaper than the neck. These methods include acting on channel information or acting on spatial information. The SPP focuses on spatial information, which is concatenated of four parallel branches: three maximum pooling operations (kernel size is 5×5, 9×9 and 13×13) and a shortcut from the input. It is used to solve the problem of the excessive object scale variations, by merging the local and global features of the inputs. The SPPF, from the YOLOv5, enhances the computational efficiency. This efficiency, η_c , increased by nearly 277.8%. And the general formula of the η_c is $[(k_1^2 + k_2^2 + k_3^2 + \dots + k_i^2 - i) - (k_1^2 - 1) \times i] \times 100\%$, where k_i is the kernel size of the i -th branch of maxpooling-2D in SPPF module. Figure 5 (a) and (b) show the structures of the SPP and SPPF.

The SE is a channel attention module, including two operation processes: the squeeze and the excitation. This module allows the networks to focus more on the more informative features channels and negatives the less informative features channels. The CBAM is a spatial-channel attention mechanism module. The CA module is a new solution to avoid the loss of positional information caused by global pooling-2D operation: to put the attention in two dimensions of width and height respectively for the efficient utilization of the spatial coordinate information of input feature maps. Figure 6 (a), (b) and (c) show the structures of the SE, CBAM and CA module. One suggestion is that the attention modules are usually placed at the end of the backbone to achieve better results, while the simple but effective SPPF module can be directly embedded at the entrance of the head. This is because the shallow networks are flooded with a large amount of low-level semantic information, resulting in the information fusion function of the attention modules being of minimal use: it is completely unnecessary to fuse feature maps that already contain rich low-level semantic information.

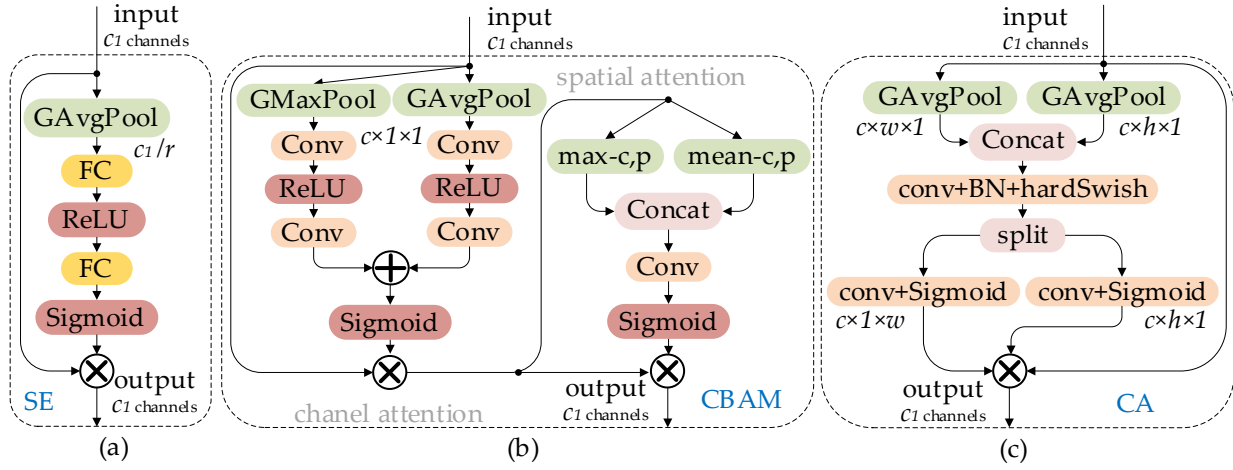


Figure 6. The structures of the three different attention modules. (a) The SE module, the character “GAvgPool” means the global average pooling-2D layer, the character “FC” means the fully connection layer, and the “r” is a reduction factor. (b) The CABM module, the character “Conv” means the ordinary convolution-2D layer, and the “max-c, p” and “mean-c, p” means the maximum-channel-pixel and average-channel-pixel. (c) The CA module, the character “BN” means the batch normalization layer and the character “hardSwish” means the hard-Swish activation layer.

3.4 The Loss and Activation

The IoU [32] loss plays a great value for the detectors based on deep learning. It makes the location of prediction bounding boxes regression more accurate. As research continues to evolve, more advanced IoU loss functions have been proposed by a number of researchers, such as GIoU [33], DIoU [34], CIoU [35] and the latest EIoU [36]. The IoU, CIoU and EIoU loss functions are defined as follows:

$$Loss_{IoU} = 1 - IoU, \quad IoU = \frac{A \cap B}{A \cup B} \quad (1)$$

$$Loss_{CIoU} = 1 - IoU + \frac{\rho_{(b,b^{gt})}^2}{d^2} + \alpha v, \quad \alpha = \frac{v}{(1 - IoU) + v}, \quad v = \frac{4}{\pi^2} (\arctan \frac{w^{gt}}{h^{gt}} - \arctan \frac{w}{h})^2 \quad (2)$$

$$Loss_{EIoU} = 1 - IoU + \frac{\rho_{(b,b^{gt})}^2}{d^2} + \frac{\rho_{(w,w^{gt})}^2}{C_w^2} + \frac{\rho_{(h,h^{gt})}^2}{C_h^2} \quad (3)$$

where the parameters “A” and “B” denote the area of ground truth bounding box and the area of prediction bounding box; the parameter “C” denotes the area of the minimum enclosing box of the ground truth bounding box and the prediction bounding box; the parameter “d” denotes the Euclidean distances of the diagonal vertices of the enclosing box; the parameter “ρ” denotes the Euclidean distances of the centroids of ground truth bounding box and prediction bounding box; the parameter “α” is an indicator for trade-off, and the parameter “v” is an indicator to evaluate the consistency of the aspect ratio of the ground truth bounding box and prediction bounding box. The CIoU loss is currently the most widely used loss function in anchor-based detector, but there are still flaws in the CIoU loss:

$$\frac{\partial v}{\partial w} = \frac{8}{\pi^2} (\arctan \frac{w^{gt}}{h^{gt}} - \arctan \frac{w}{h}) \times \frac{h}{w^2 + h^2}, \quad \frac{\partial v}{\partial h} = -\frac{8}{\pi^2} (\arctan \frac{w^{gt}}{h^{gt}} - \arctan \frac{w}{h}) \times \frac{w}{w^2 + h^2}$$

where the “ $\frac{\partial v}{\partial w}$ ” is the gradient of the “v” with respect to the “w”, the “ $\frac{\partial v}{\partial h}$ ” is the gradient of the “v” with respect to the “h.”

According to the definition of the CIoU loss, if $\{(w = kw^{gt}, h = kh^{gt}) | k \in R^+\}$, the CIoU loss will degenerate into the DIoU loss, i.e., the relative proportion of penalty terms added in the CIoU loss (αv) will not work [36]. Further, the $\frac{\partial v}{\partial w}$ and the $\frac{\partial v}{\partial h}$ have opposite signs, $\frac{\partial v}{\partial w} = -(h/w) \times (\frac{\partial v}{\partial h})$. Thus, these two variables (w or h) can only be updated in the same direction, increasing or decreasing at the same time. This is not in line with practical application scenarios especially when $w < w^{gt}$ and $h < h^{gt}$ or $w > w^{gt}$ and $h > h^{gt}$. The EIoU loss does not face such a problem, it directly uses the w and h of a prediction bounding box independently for the penalty term, instead of the ratio of the w and h. The bounding box

regression method of the EIoU is more exact especially when the object’s width and height lengths differ greatly.

On deep networks, the accuracy and training stability of the models using Swish [37] and Mish [38] are generally better than ReLU [39]. Both the Swish and Mish have the properties of no upper bound with lower bound, smooth, and non-monotonic. They are defined as follows:

Swish: $f(x) = x \cdot \text{sigmoid}(\beta x)$ (4); Mish: $f(x) = x \cdot \tanh(\log(1 + e^x))$ (5)

The Mish performs slightly better for model accuracy than Swish on deeper networks, although in fact the two activation function curves are so close. Compared with the Swish, the Mish consumes more training time because of the increase in computational cost. We performed adequate ablation experiments to verify the effectiveness of these methods. The comparative analyses are reported in Table 7.

4. Experiments and Analysis

We use the Pytorch framework to build the models. All the models are trained with two Nvidia Tesla T4 or one Nvidia A40 at Linux CentOS 7 operating system. The hyper-parameters are as follows: the training steps is 33000; the optimizer is stochastic gradient descent; the batch size is 128; the linear decay learning rate scheduling strategy is adopted with initial learning rate 0.01 and final 0.001; the warm-up steps is 1000; the momentum and weight decay are 0.937 and 0.0005. All the validation experiments are performed on a Tesla T4 or a Jetson Nano. The Jetson Nano’s operation system is Linux Ubuntu 18.04. In tables and figures, the mAP_{0.5} is the average precision of the all categories when the accuracy evaluation IoU threshold is set to 0.5 and mAP_{0.95} is the average precision with the IoU threshold taken in steps of 0.05 from 0.5 to 0.95 and weighted average.

4.1 Data Sets

We use the publicly available data sets WiderPerson [40], PASCAL VOC [41], SODA10M [42] and DOTA1.0 [44]. We choose the WiderPerson to evaluate the practical effects of the GSConv method and the different attention modules. It is a pedestrian detection benchmark dataset in the wild, of which images are selected from a wide range of scenarios, no longer limited to the traffic scenario. The images collected in this dataset are all in a dense crowded environment with a large number of pedestrians and serious overlap and mutual occlusion. And, we use the PASCAL VOC 2007+12 to compare with the state-of-the-art lightweight models. Ultimately, we use the SODA10M to test the real-world performance of these models in a traffic environment. We test the evolved models on a Jetson Nano, and on the low-power edge devices we expect these models to be competent for the use cases in embedded or IoT scenarios.

4.2 Ablation Studies

In Table 3, we tested the accuracy of the YOLOv5n detectors constructed with five different convolution methods (using the same hyperparameters for fairness) on the PASCAL VOC 2007+12 dataset. These methods include the SC, the DSC, the ShuffleNet method, the GhostNet method and the GSConv. We use the different methods at down-sample scales of 1/8, 1/16 and 1/32 in the backbone in order to verify more clearly the differences in the effectiveness of the five methods. The best outcomes obtained by GSConv with the less time complexity in the end. In Table 4, we compare the performances, including accuracy, complexity, and inference time of one batch size on CPU (Intel Xeon Gold 5118) and GPU (T4), of two shuffle approaches for the GSConv. In the results, the transposition approach is more competitive in comparison items, while linear fusion approach is a substitute when the transposition is not supported on some devices. In Table 6, we reported the experimental results of the employing different attention modules by the YOLOv5n. All the models in the part I use the slim-neck with slim-backbone, and the models in the part II only use the slim-neck. The experimental datasets are the WiderPerson and VOC 2007+12. In this Table, the "SE*3 640" indicates that the SE module is used three times and SPPF once in the YOLOv5n’s structure, and the training image size is 640×640 pixels.

Table 3. The comparisons of the feature extraction capability and time complexity of the SC, DSC, ShuffleNet method, GhostNet method and GSConv (PASCAL VOC 2007+12 dataset).

Convolutional-block methods	mAP _{0.5}	mAP _{0.95}	Complexity (FLOPs)
SC	58.9%	35.8%	4.2G
DSC	56.9%	34.6%	3.3G
ShuffleNet method	56.5%	34.1%	3.3G
GhostNet method	59.3%	37.0%	3.8G
GSConv (ours)	59.8%	38.1%	3.7G

Table 4. The comparisons of two shuffle approaches for the GSConv (PASCAL VOC 2007+12 dataset).

shuffle options	mAP _{0.5}	mAP _{0.95}	FLOPs	Latency _{CPU}	Latency _{GPU}
Transposition operating	59.8%	38.1%	3.7G	37.8ms	4.3ms
linear operating (no B.N)	59.5%	38.0%	3.7G	38.6ms	4.4ms
linear + B.N.	59.9%	38.2%	3.9G	39.0ms	4.4ms
nonlinear operating (+ ReLU)	60.2%	39.6%	3.7G	38.0ms	4.8ms

Table 5. The comparisons of three different VoV-GSCSP modules for the slim neck yolov5n (PASCAL VOC 2007+12 dataset).

modules	mAP _{0.5}	mAP _{0.95}	FLOPs	Latency _{b=1}	FPS
VoV-GSCSP ₁	61.1%	39.3%	4.1G	4.5ms	168
VoV-GSCSP ₂	60.6%	39.2%	4.2G	4.7ms	164
VoV-GSCSP ₃	60.8%	36.8%	4.3G	4.9ms	160

Table 6. The performance comparisons of employment of different attention modules (GPU: T4).

Attentions	Param.	P. & R.	mAP _{0.5}	mAP _{0.95}	Latency _{b=64}	FLOPs
Part I. slim-backbone + slim-neck						
WiderPerson _{single class: pedestrian}						
SE*3 ₆₄₀	0.664M	63.5%, 78.8%	79.9%	46.4%	2.2ms	1.7G
CBAM*3 ₆₄₀	0.664M	63.8%, 79.0%	79.9%	46.4%	2.3ms	1.7G
CA*3 ₆₄₀	0.665M	56.6%, 82.0%	80.4%	47.1%	2.2ms	1.7G
PASCAL VOC 2007+12 _{20 classes}						
SE*3 ₆₄₀	0.685M	57.3%, 52.3%	51.4%	27.5%	2.3ms	1.8G
CBAM*3 ₆₄₀	0.685M	59.8%, 51.1%	51.2%	27.7%	2.4ms	1.8G
CA*3 ₆₄₀	0.685M	58.5%, 52.3%	52.1%	28.6%	2.3ms	1.8G
Part II. slim-neck only						
WiderPerson _{single class: pedestrian}						
SE*3 ₆₄₀	1.14M	62.3%, 82.9%	82.7%	50.6%	1.7ms	3.5G
CBAM*3 ₆₄₀	1.14M	64.1%, 81.4%	82.1%	49.9%	1.9ms	3.5G
CA*3 ₆₄₀	1.14M	60.5%, 84.4%	83.3%	51.5%	1.9ms	3.5G
PASCAL VOC 2007+12 _{20 classes}						
SE*3 ₆₄₀	1.17M	64.2%, 56.9%	59.2%	37.6%	2.2ms	3.5G
CBAM*3 ₆₄₀	1.17M	61.4%, 58.2%	58.7%	36.8%	2.3ms	3.5G
CA*3 ₆₄₀	1.17M	64.2%, 57.5%	59.3%	38.3%	2.3ms	3.5G

We found that the effect of different attention modules on the number of parameters and inference time of the detector is so slight as to be almost negligible but the impact on the accuracy is significant: the “CA*3+SPPF*1” model obtains the best results with the same number of parameters on the VOC 2007+12 and WiderPerson datasets. In addition, the accuracy of the slim-neck model is much better than that of the slim-backbone-neck when the inference time is very close. If we force to close the accuracy of the slim-neck model and the slim-neck-backbone model, the latter needs to spend more than 3.5% inference time.

Further, we conducted comparative experiments on the effects of Mish and Swish activation functions, as well as CIoU and EIoU loss functions for accuracy and speed. In [Table 7](#), we reported the experimental results on the VOC 2007+12 dataset. The networks using Mish with EIoU achieve the higher average accuracy, while the networks using Swish achieve the faster speed (training time using the Mish increases by about 29.26% than Swish). For contrast intuitive, we validated the effectiveness of our method with YOLOv5n as a baseline, and [Table 8](#) reported the relevant experiment results.

Table 7. The comparison of the effects of Swish/Mish activation functions and CIoU/EIoU loss functions (GPU: T4; dataset: PASCAL VOC 2007+12).

Attentions	Act. / Bbox_Loss	mAP _{0.5}	mAP _{0.95}	Latency _{b=1}	FPS
CA*3, SPPF*1 ₆₄₀ (slim-neck only)	Swish, CIoU	59.3%	38.3%	5.8ms	136.4
	Swish, EIoU	59.7%	38.5%	5.7ms	138.4
	Mish, CIoU	60.0%	38.4%	7.0ms	119.0
	Mish, EIoU	60.6%	39.1%	7.2ms	116.3

Table 8. The ablation studies of three implements: the slim-neck, attention modules, and activation & loss functions (GPU: T4; dataset: PASCAL VOC 2007+12). Models marked ‘*’ are using the VoV-GSCSP₁ and marked ‘*’ are using the cheaper VoV-GSCSP₁ (a DWConv layer to replace a Conv layer in the GS bottleneck module). Note that it is possible to obtain different FPS for the same Latency due to differences in post-processing time (NMS) between different models.

Models	Param., FLOPs	mAP _{0.5}	mAP _{0.95}	Latency _{b=1}	FPS
Baseline (YOLOv5n)	1.79M, 4.3G	58.0%	35.0%	5.8ms	136.8
Baseline + slim-backbone-neck *	0.67M(-63%), 1.8G	51.5%(-6.5)	27.9%(-8.1)	5.0ms	151.9
Baseline + slim-backbone-neck (deep) *	1.23M(-31%), 4.0G	61.1%(+3.1)	39.7%(+4.7)	6.0ms	132.7
Baseline + slim-neck *	1.15M(-36%), 3.5G	58.9%(+0.9)	37.1%(+2.1)	4.8ms	155.4
Baseline + slim-neck *	1.68M(-0.6%), 4.1G	61.1%(+3.1)	39.3%(+4.3)	4.8ms	168.9
Baseline + slim-neck, CA*3, Mish, EIoU *	1.17M(-36%), 3.5G	60.6%(+2.6)	39.1%(+4.1)	7.2ms	116.3
Baseline + slim-neck, SPPF*4, CA*3, Mish, CIoU *	1.38M(-23%), 3.8G	61.0%(+3.0)	39.0%(+4.0)	7.2ms	118.6
Baseline + slim-neck, SPPF*4, CA*3, Mish, EIoU *	1.38M(-23%), 3.8G	62.2%(+4.2)	41.5%(+6.5)	7.4ms	115.0
Baseline + slim-neck, SPPF*4, CA*3, Mish, EIoU *	1.91M(+0.06%), 4.6G	64.5%(+6.3)	43.9%(+8.9)	7.6ms	112.4

4.3 Comparisons between the Slim-neck detectors and the Originals

Finally, we give the performance comparisons of the slim-neck YOLO detectors and the originals in [Table 9](#). The slim-neck detectors achieve the best accuracy with the smaller size. The combination of the slim-neck method and the tricks makes a huge improvement on the accuracy, especially to the lightweight detectors such as the YOLOv3/v4-tiny. And we put slim-neck tiny detectors on the Jetson Nano embedded device for inferring with 320×320 pixels, results listed in [Table 10](#). In [Figure 7](#), we compare the speed and accuracy of five SOTA detectors on the driverless dataset of the SODA10M. We test the effectiveness of our approach using a 20-second field video that was captured by a dash cam at night in low-light. In [Figure 8](#), we show four frames from the test video as an intuitive comparison.

Table 9. The comparisons of the detectors based on slim neck and the originals of the different state-of-the-art lightweight detectors (GPU: T4; dataset: PASCAL VOC 2007+12).

Detectors	Param., FLOPs	mAP _{0.5}	mAP _{0.95}	Latency _{b=1}	FPS
Originals:					
YOLOv3-tiny	8.71M, 13.0G	42.5%	18.5%	3.2ms	202.5
YOLOv4-tiny	6.11M, 17.6G	45.3%	21.3%	3.7ms	178.6
YOLOv5n	1.79M, 4.3G	58.0%	35.0%	5.8ms	136.8
MobileNetv3-YOLOv5s	3.59M, 6.4G	55.3%	32.6%	6.7ms	121.4
ShuffleNetv2-YOLOv5s	5.56M, 11.6G	56.1%	35.4%	5.0ms	151.3
GhostNet-YOLOv5s	3.73M, 8.2G	63.0%	42.1%	6.0ms	135.1
Slim neck by GSConv (ours approach):					
slim-neck YOLOv3-tiny	5.86M, 9.6G	56.8%(+14.3)	33.6%(+15.1)	3.0ms	219.5
slim-neck YOLOv4-tiny	5.66M, 16.2G	61.3%(+16.0)	37.3%(+16.0)	3.7ms	179.1
slim-neck YOLOv5n	1.15M, 3.5G	58.9%(+0.9)	37.1%(+2.1)	4.8ms	155.4
GSConv-MobileNetv3-YOLOv5s	9.30M, 14.1G	61.9%(+6.6)	41.4%(+8.8)	8.3ms	102.9
GSConv-ShuffleNetv2-YOLOv5s	7.74M, 13.6G	58.7%(+2.6)	37.9%(+2.5)	5.8ms	137.1
GSConv-GhostNet-YOLOv5s	3.73M, 8.2G	63.6%(+0.6)	42.8%(+0.7)	6.8ms	122.8

Table 10. The performances of the slim-neck tiny detectors on the Jetson Nano (dataset: PASCAL VOC 2007+12).

Detectors	FLOPs	mAP _{0.5}	Latency _{FP16, b=4}	FPS
-----------	-------	--------------------	------------------------------	-----

slim-neck YOLOv3-tiny	9.6G	50.8%	30.1ms	108.6
slim-neck YOLOv4-tiny	16.2G	56.8%	36.0ms	91.4

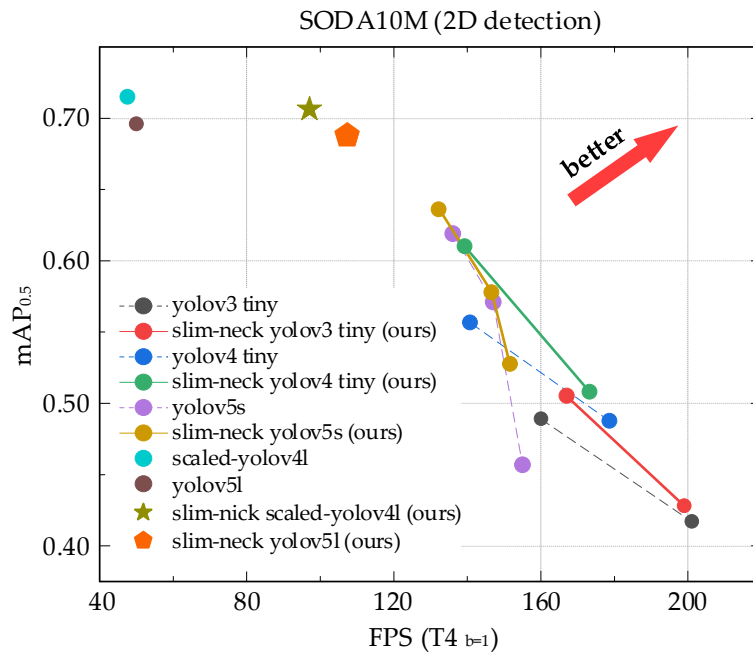


Figure 7. The comparison of the slim-neck YOLO family detectors and the originals (the FP16 used to inference the slim-neck scaled-yolov4l and slim-neck yolov5l).



Figure 8. The visual results of the slim-neck approach in the field traffic (by a Jetson nano).

5. Discussion

At present, there are mainly two types of object detectors based on deep learning, Transformer-based and CNNs-based. The application of Transformer-based detectors faces hardship due to the bad latency and the CNNs-based detectors are still the preferred option in the industry. Researchers have proposed numerous approaches to further optimize the performance of CNNs-based models. Our proposed GSConv

provides researchers with a new design option for CNNs-based detectors or classifiers. For lightweight models, designers can directly replace the original convolutional layers with GSConv layers to obtain significant accuracy gains without additional operations. In fact, we have tested the GSConv in some vision-based specific assisted driving systems, such as a height-limited collision monitoring and warning system for trucks. The results are promising. But it is worth noting that the advantages of the GSConv become less obvious as the computing power of the platform grows. The GSConv is more suitable for edge computing devices because of the small computational consumption and memory footprint. In brief, if both cost and performance of the model are considered, it would be a wise choice to adopt the GSConv.

6. Conclusions

To sum up, in this paper we introduce a new lightweight convolution method, the GSConv, to allow the depth-wise separable convolution to achieve the close effects to the vanilla convolution and more efficient. And we design the one-shot aggregation module, VoV-GSCSP, to replace the ordinary bottleneck module to speed up inference. Further, we provide the slim-neck design paradigm for lightweight. In our experiments, the GSConv shows the better performance compared to the other lightweight convolution methods. And with our approach, the tested detectors throw away 7.2%~32.7% of the computational cost but obtain 1.2%~35.3% improvement of the accuracy and the given results outperform state-of-the-art detectors’.

Acknowledgments: The authors would like to thank Ms. Xinxin Liu for her aid of the experimental platform providing.

Data Availability

Publicly available data sets:

1. the WiderPerson at <http://www.cbsr.ia.ac.cn/users/sfzhang/WiderPerson/>
 2. the PASCAL VOC 2012 at <http://host.robots.ox.ac.uk/pascal/VOC/voc2012/>
 3. the SODA10M at <https://soda-2d.github.io/index.html>
 4. the DOTA1.0 at <http://captain.whu.edu.cn/DOTAweb>
- Code of this paper is available at <https://github.com/alanli1997/slim-neck-by-gsconv>

Appendix

A. The comparisons of the FLOPs and parameters amount between the DSC and SC

The effect of DSC is obvious in the reduction of the parameters number to detection networks. The parameters’ amount to a conventional convolutional layer is $C_1 \times K_1 \times K_2 \times C_2$, and the amount for a DSC layer is $C_1 \times K_1 \times K_2 + 1 \times 1 \times C_1 \times C_2$, where C_1 and C_2 are the channels number of the feature maps from input and output, and $K_1 \times K_2$ is the kernel size of convolutional. The calculation cost to a conventional convolution layer is $W \times H \times C_1 \times K_1 \times K_2 \times C_2$, and the cost to a DSC’s is $W \times H \times C_1 \times K_1 \times K_2 + W \times H \times 1 \times 1 \times C_1 \times C_2$, where W and H are the width and height of the feature maps. The reason of DSC operation is cheaper than conventional convolutional can be explained by assuming the following conditions:

$$\left\{ \begin{array}{l} size_{input} = W \times H \times C_1 = 320 \times 320 \times 3 \\ size_{output} = W \times H \times C_2 = 320 \times 320 \times 16 \\ size_{kernel} = K_1 \times K_2 = 3 \times 3 \\ ratio_p = \frac{C_1 \times K_1 \times K_2 + 1 \times 1 \times C_1 \times C_2}{C_1 \times K_1 \times K_2 \times C_2} = \frac{1}{C_2} + \frac{1}{K_1 \times K_2} \approx 0.174 \\ ratio_c = \frac{W \times H \times C_1 \times K_1 \times K_2 + W \times H \times 1 \times 1 \times C_1 \times C_2}{W \times H \times C_1 \times K_1 \times K_2 \times C_2} \\ = \frac{1}{C_2} + \frac{1}{K_1 \times K_2} \approx 0.174 \end{array} \right.$$

where the $ratio_p$ is a ratio of the parameters amount, between DSC and conventional convolutional layer, and the $ratio_c$ is a ratio of the calculation cost of them. Obviously, the DSC's parameters amount and the calculation cost are indeed less and much lower than SC's.

B. The slim neck structures of the scaled-YOLOv4 and YOLOv5

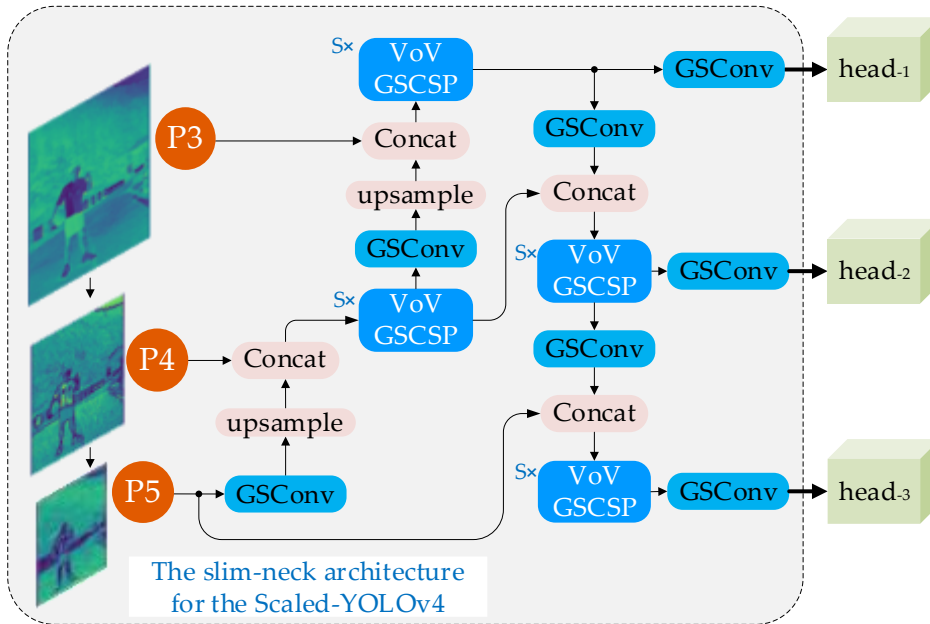


Figure a. The slim-neck architecture for the Scaled-YOLOv4(p5).

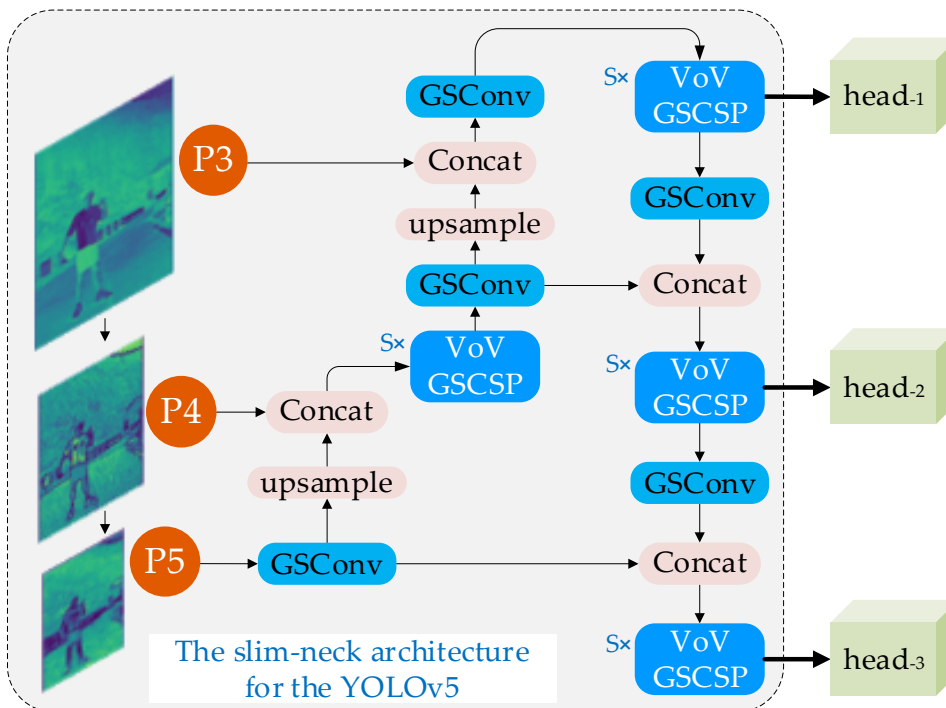


Figure b. The slim-neck architecture for the YOLOv5.

C. Comparison of remote sensing image detection

We train the scaled-YOLOv4 and the Slim neck scaled-YOLOv4 with an A40 on DOTA1.0 (Using the same hyperparameters) to compare the ability of the two detectors to detect small objects. Figure (c) and (d) show the test results, and the source image is from the 23rd image of the test set of the ITCVD dataset (<https://eostore.itc.utwente.nl:5001/fsdownload/zZYfgbB2X/ITCVD>).

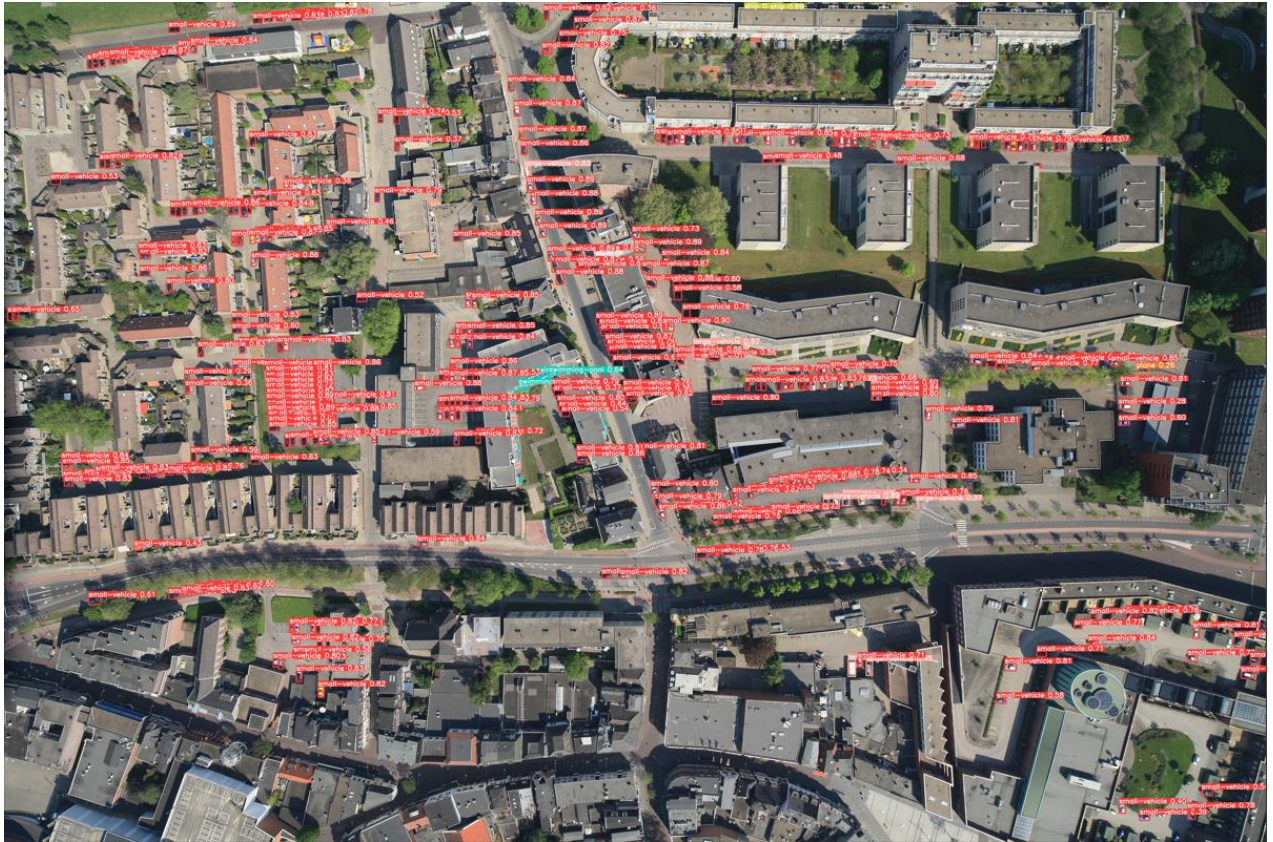


Figure c. The detection result of the slim-neck scaled YOLOv4l.



Figure d. The detection result of the original scaled YOLOv4l.

References

1. R. Girshick; J. Donahue; T. Darrell; J. Malik. Rich feature hierarchies for accurate object detection and semantic segmentation. in Proc. IEEE Comput. Soc. Conf. Comput. Vis. Pattern Recognit. (CVPR), Columbus, OH, USA 23-28 June 2014; pp. 580-587. DOI: 10.1109/CVPR.2014.81
2. R. Girshick. Fast R-CNN. Proc. IEEE Int. Conf. Comput. Vis. (ICCV), Santiago, Chile 07-13 December 2015; pp. 1440-1448. DOI: 10.1109/ICCV.2015.169
3. S. Ren; K. He; R. Girshick; J. Sun. Faster R-CNN: Towards real-time object detection with region proposal networks. IEEE Trans Pattern Anal. Mach. Intel. 2017, 39, 6, 1137-1149. DOI: 10.1109/TPAMI.2016.2577031
4. J. Redmon; S. Divvala; R. Girshick; and A. Farhadi. You only look once: Unified, real-time object detection. in Proc. IEEE Conf. Comput. Vis. Pattern Recog. (CVPR), Las Vegas, NV, USA 27-30 June 2016; pp. 779-788. DOI: 10.1109/CVPR.2016.91
5. J. Redmon; A. Farhadi. YOLO9000: better, faster, stronger. in Proc. IEEE Conf. Comput. Vis. Pattern Recog. (CVPR), Honolulu, HI, USA 21-26 July 2017; pp. 6517-6525, arXiv:1612.08242. [Online]. Available: <https://arxiv.org/abs/1612.08242v1> DOI: 10.1109/CVPR.2017.690
6. J. Redmon; A. Farhadi. YOLOv3: An incremental improvement. arXiv eprints 2018, arXiv:1804.02767. [Online]. DOI: <https://arxiv.org/abs/1804.02767>
7. A. Bochkovskiy; C. Y. Wang; H-Y. M. Liao. Yolov4: Optimal speed and accuracy of object detection. in Proc. IEEE Conf. Comput. Vis. Pattern Recog. (CVPR), Apr. 2020, arXiv:2004.10934. [Online] DOI : <https://arxiv.org/abs/2004.10934>
8. W. Liu; D. Anguelov; D. Erhan; C. Szegedy; Scott Reed; C. Y. Fu; A. C. Berg. SSD: Single shot multibox detector. in Proc. Eur. Conf. Comput. Vis. (ECCV), Sep. 2016, pp. 21-37. DOI: https://doi.org/10.1007/978-3-319-46448-0_2
9. C. Y. Fu; W. Liu; A. Ranga; A. Tyagi; A. C. Berg. DssD: Deconvolutional single shot detector. arXiv eprints 2017, arXiv:1701.06659. [Online]. Available: <https://arxiv.org/abs/1701.06659> DOI: <https://doi.org/10.48550/arXiv.1701.06659>
10. F. Chollet. Xception: Deep learning with depthwise separable convolutions. in Proc. IEEE Conf. Comput. Vis. Pattern Recog. (CVPR), Honolulu, HI, USA 21-26 July 2017; pp. 1800-1807. [Online]. Available: <https://arxiv.org/abs/1610.02357v1> DOI: 10.1109/CVPR.2017.195
11. A. G. Howard; M. Zhu; B. Chen; D. Kalenichenko; W. Wang; T. Weyand; M. Andreetto; A. Hartwig. Mobilenets: Efficient convolutional neural networks for mobile vision applications. arXiv eprints 2017, arXiv:1704.04861. [Online]. Available: <https://arxiv.org/abs/1704.04861>
12. M. Sandler; A. Howard; M. Zhu; A. Zhmoginov; L. Chen. Mobilenetv2: Inverted residuals and linear bottlenecks. in Proc. IEEE Conf. Comput. Vis. Pattern Recog. (CVPR), Jun. 2018, arXiv:1801.04381. [Online]. Available: <https://arxiv.org/abs/1801.04381v4> DOI: 10.1109/CVPR.2018.00474
13. A. Howard; M. Sandler; G. Chu; L. Chen; B. Chen; M. Tan; W. Wang; Y. Zhu; R. Pang; V. Vasudevan; Q. V. Le; H. Adam. Searching for MobileNetV3. in Proc. IEEE Int. Conf. Comput. Vis. (ICCV), Apr. 2019, arXiv:1704.04861. [Online]. Available: <https://arxiv.org/abs/1704.04861> DOI: 10.1109/ICCV.2019.00140
14. X. Zhang; X. Zhou; M. Lin; J. Sun. ShuffleNet: An extremely efficient convolutional neural network for mobile devices. in Proc. IEEE Conf. Comput. Vis. Pattern Recog. (CVPR), Jul. 2017, arXiv:1707.01083. [Online]. Available: <https://arxiv.org/abs/1707.01083v1> DOI: 10.1109/CVPR.2018.00716
15. N. Ma; X. Zhang; H. Zheng; J. Sun. ShuffleNet V2: Practical guidelines for efficient CNN architecture design. in Proc. Eur. Conf. Comput. Vis. (ECCV), Jul. 2018, arXiv:1807.11164. [Online]. Available: <https://arxiv.org/abs/1807.11164v1> DOI: https://doi.org/10.1007/978-3-030-01264-9_8
16. K. Han; Y. Wang; Q. Tian; J. Guo; C. Xu; C. Xu. GhostNet: More features from cheap operations. in Proc. IEEE Conf. Comput. Vis. Pattern Recog. (CVPR), Mar. 2020, arXiv:1911.11907. [Online]. Available: <https://arxiv.org/abs/1911.11907> DOI: 10.1109/CVPR42600.2020.00165
17. A. Krizhevsky; I. Sutskever; G. E. Hinton. ImageNet classification with deep convolutional neural networks. Association for Computing Machinery 2012; 25, pp. 84-90. DOI: <https://doi.org/10.1145/3065386>

18. K. Simonyan; A. Zisserman. Very deep convolutional networks for large-scale image recognition. CoRR 2015; arXiv:1409.1556. [Online]. Available: <https://arxiv.org/abs/1409.1556>
19. K. He; X. Zhang; S. Ren; J. Sun. Deep residual learning for image recognition. in Proc. IEEE Conf. Comput. Vis. Pattern Recog. (CVPR), Jun. 2016, pp. 770-778. DOI: 10.1109/CVPR.2016.90
20. T. -Y. Lin; P. Dollár; R. Girshick; K. He; B. Hariharan; S. Belongie. Feature pyramid networks for object detection. in Proc. IEEE Conf. Comput. Vis. Pattern Recog. (CVPR), Honolulu, HI, USA 21-26 July 2017; pp. 936-944. DOI: 10.1109/CVPR.2017.106
21. Z. Tian; C. Shen; H. Chen; T. He. FCOS: Fully Convolutional One-Stage Object Detection. International Conference on Computer Vision. (ICCV), Seoul, Korea (South) 27 October 2019 - 02 November 2019; pp. 9626-9635. DOI: 10.1109/ICCV.2019.00972
22. C. Zhu; Y. He; M. Savvides. Feature selective anchor-free module for single-shot object detection. in Proc. IEEE Conf. Comput. Vis. Pattern Recog. (CVPR), Long Beach, CA, USA 15-20 June 2019; pp. 840-849. DOI: 10.1109/CVPR.2019.00093
23. A. Neubeck; L. Van Gool. Efficient non-maximum suppression. 18th International Conference on Pattern Recognition. (ICPR'06), Hong Kong, China 20-24 August 2006; pp. 850-855. DOI: 10.1109/ICPR.2006.479
24. C. -Y. Wang; A. Bochkovskiy; H. -Y. M. Liao. Scaled-yolov4: Scaling cross stage partial network. in Proc. IEEE Conf. Comput. Vis. Pattern Recog. (CVPR), Nashville, TN, USA, 20-25 June 2021; pp. 13024-13033. DOI: 10.1109/CVPR46437.2021.01283
25. K. He; X. Zhang; S. Ren; J. Sun. Spatial pyramid pooling in deep convolutional networks for visual recognition. in IEEE Transactions on Pattern Analysis and Machine Intelligence, vol. 37, no. 9, pp. 1904-1916, Sept. 2015. DOI: 10.1109/TPAMI.2015.2389824
26. J. Hu; L. Shen; S. Albanie; G. Sun; E. Wu. Squeeze-and-excitation networks. IEEE Transactions on Pattern Analysis and Machine Intelligence (Volume: 42, Issue: 8, 01 August 2020) [Online]. Available: <https://arxiv.org/abs/1709.01507v4> DOI: 10.1109/TPAMI.2019.2913372
27. S. Woo, J. Park; J. Lee; I. S. Kweon. CBAM: Convolutional block attention module. in Proc. Eur. Conf. Comput. Vis. (ECCV), Jul. 2018, arXiv:1807.06521. [Online]. Available: <https://arxiv.org/abs/1807.06521v1> DOI: https://doi.org/10.1007/978-3-030-01234-2_1
28. Q. Hou, D. Zhou; J. Feng. Coordinate attention for efficient mobile network design. in Proc. IEEE Conf. Comput. Vis. Pattern Recog. (CVPR), Jun. 2021, arXiv:2103.02907. [Online]. Available: <https://arxiv.org/abs/2103.02907> DOI: 10.1109/CVPR46437.2021.01350
29. G. Huang; Z. Liu; L. Van Der Maaten; K. Q. Weinberger. Densely connected convolutional networks. in Proc. IEEE Conf. Comput. Vis. Pattern Recog. (CVPR), Honolulu, HI, USA 21-26 July 2017; pp. 2261-2269. DOI: 10.1109/CVPR.2017.243
30. Y. Lee; J. -w. Hwang; S. Lee, Y. Bae; J. Park. An energy and GPU-computation efficient backbone network for real-time object detection. 2019 IEEE/CVF Conference on Computer Vision and Pattern Recognition Workshops (CVPRW), Long Beach, CA, USA 16-17 June 2019; pp. 752-760. DOI: 10.1109/CVPRW.2019.00103
31. C. -Y. Wang; H. -Y. Mark Liao; Y. -H. Wu; P. -Y. Chen; J. -W. Hsieh; I. -H. Yeh. CSPNet: A new backbone that can enhance learning capability of CNN. 2020 IEEE/CVF Conference on Computer Vision and Pattern Recognition Workshops (CVPRW), Seattle, WA, USA 14-19 June 2020; pp. 1571-1580. DOI: 10.1109/CVPRW50498.2020.00203
32. J. Yu; Y. Jiang; Z. Wang; Z. Cao; T. Huang. UnitBox: An advanced object detection network. Association for Computing Machinery, New York, NY, USA Oct. 2016; pp. 516-520. DOI: <https://doi.org/10.1145/2964284.2967274>
33. H. Rezatofighi; N. Tsoi; J. Gwak; A. Sadeghian; I. Reid; S. Savarese. Generalized intersection over union: A metric and a loss for bounding box regression. in Proc. IEEE Conf. Comput. Vis. Pattern Recog. (CVPR), Jun. 2019; pp. 658-666. DOI: 10.1109/CVPR.2019.00075
34. Z. Zheng; P. Wang; W. Liu; J. Li; R. Ye; D. Ren. Distance-IoU Loss: Faster and better learning for bounding box regression. In Proceedings of the AAAI Conference on Artificial Intelligence (AAAI), Apr. 2020, 34, 7; pp. 12993-13000. DOI: <https://doi.org/10.1609/aaai.v34i07.6999>

35. Z. Zheng; P. Wang; D. Ren; W. Liu; R. Ye; Q. Hu; W. Zuo. Enhancing geometric factors in model learning and inference for object detection and instance segmentation. in *IEEE Transactions on Cybernetics*, 2021, pp. 1-13, doi: 10.1109/TCYB.2021.-3095305. DOI: 10.1109/TCYB.2021.3095305
36. Y. Zhang; W. Ren; Z. Zhang; Z. Jia; L. Wang; T. Tan. Focal and efficient IoU loss for accurate bounding box regression. *arXiv eprints 2021*, arXiv:2101.08158 2021. [Online]. Available: <https://arxiv.org/abs-/2101.08158> DOI: <https://doi.org/10.1016/j.neucom.2022.07.042>
37. P. Ramachandran; B. Zoph; Q. V. Le. Searching for activation functions. *arXiv eprints 2017*, arXiv:1710.05941. [Online]. DOI: <https://doi.org/10.48550/arXiv.1710.05941>
38. D. Misra. Mish: A self regularized non-monotonic activation function. *arXiv eprints 2020*, arXiv:1908.08681. [Online]. DOI: <https://arxiv.org/abs/1908.08681>
39. X. Glorot; A. Bordes; Y. Bengio. Deep sparse rectifier neural networks. *Proceedings of the fourteenth international conference on artificial intelligence and statistics*, 2011, 15, pp. 315-323. DOI: <https://doi.org/10.1.1.208.6449>
40. S. Zhang; Y. Xie; J. Wan; H. Xia; S. Z. Li; G. Guo. WiderPerson: A diverse dataset for dense pedestrian detection in the wild. in *IEEE Transactions on Multimedia*, 2020, 22, 2, pp. 380-393. DOI: 10.1109/TMM.2019.2929005
41. M. Everingham; S. M. Ali Eslami; L. V. Gool; C. K. I. Williams; J. Winn; A. Zisserman. The PASCAL Visual Object Classes Challenge: A Retrospective. *International Journal of Computer Vision* 2015; 111, pp. 98–136. DOI: <https://doi.org/10.1007/s11263-014-0733-5>
42. J. Han; X. Liang; H. Xu; K. Chen; L. Hong; C. Ye; W. Zhang; Z. Li; X. Liang; C. Xu. Soda10m: Towards large-scale object detection benchmark for autonomous driving. *arXiv eprints 2021*, arXiv: 2106.11118. DOI: <https://doi.org/10.48550/arXiv.2106.11118>
43. J. Glenn. Yolov5, 2022, <https://github.com/ultralytics/yolov5>
44. Gui-Song Xia; Xiang Bai; Jian Ding; Zhen Zhu; Serge Belongie; Jiebo Luo; Mihai Datcu; Marcello Pelillo; Liangpei Zhang. DOTA: A Large-Scale Dataset for Object Detection in Aerial Images. *2018 IEEE/CVF Conference on Computer Vision and Pattern Recognition 2018*, Salt Lake City, UT, USA. DOI: 10.1109/CVPR.2018.00418